Linear and Nonlinear Characterizations of Chalcogenide Photonic Crystal Fibers

Julien Fatome, Coraline Fortier, Thanh Nam Nguyen, Thierry Chartier, Frederic Smektala, Khalida Messaad, Bertrand Kibler, Stephane Pitois, Gregory Gadret, Christophe Finot, Johann Troles, Frederic Desevedavy, Patrick Houizot, Gilles Renversez, Laurent Brilland, and Nicholas Traynor

***Abstract*—In this paper, we investigate the linear and nonlinear properties of GeSbS and AsSe chalcogenide photonic crystal fibers. Through several experimental setups, we have measured the second- and third-order chromatic dispersion, the effective area, losses, birefringence, the nonlinear Kerr coefficient as well as Brillouin and Raman scattering properties.**

***Index Terms*—Chalcogenide optical fiber, microstructured optical fiber, nonlinear optics.**

I. Introduction

PHOTONIC CRYSTAL FIBERS (PCFs) are particularly attractive since they offer the possibility to significantly enhance the nonlinearity of the bulk medium by means of a strong light confinement of the electromagnetic field [1], [2]. Another advantage is the ability to tailor the material dispersion by adjusting the waveguide dispersion design. Consequently, a wide range of applications has strongly benefited from these remarkable features to generate octave-spanning optical supercontinuum [3], for biology [4] or optical metrology [5], to process nonlinear effects with high efficiency and compactness [6], and even to levitate particles [7]. Nevertheless, silica PFCs have a limited nonlinearity because of the weak nonlinear index of silica and more importantly, their intrinsic losses ban any application beyond 2 μm. Therefore, nonsilica glass PCFs have to be considered in order to enhance the field of applications of microstructured optical fibers [8]–[20]. Several glasses have been found to be very attractive for their nonlinear characteristics including chalcogenide, bismuth, tellurite or lead silicate glasses which nonlinear index are over two to three orders of magnitude higher than fused silica [9]–[16]. Despite the fact that the material dispersion of these glasses is often very large, around 1.5 μm, several results have demonstrated that a PCF design allows to shift significantly the fiber zero-dispersion towards lower wavelengths [10]–[12]. A relevant illustration of powerful nonlinear compactness and PCF dispersion shift of this nonsilica PCFs was reported in [11] in which a 4-μm bandwidth supercontinuum has been generated thanks to a 8-mm-long sample of tellurite PCF. On the other hand, chalcogenide glasses offer one of the strongest glass nonlinearity (up to 500 times silica) and has been studied in several works and applications [13]–[28]. Eggleton *et al.* have recently demonstrated a high compactness 160-Gb/s demultiplexing device and a supercontinuum generation by means of a chalcogenide fiber taper which nonlinearity reaches 80 000 times that of fused silica [13]–[15]. Recently, we have also investigated the Brillouin and Raman properties of a PCF chalcogenide fiber and shown Brillouin and Raman gains 100 and 180 larger than fused silica which underlines the potential of this kind of fiber for amplification or slow/fast light applications [17], [18].

In this paper, we review recent progress in the fabrication of chalcogenide microstructured fibers. We will present, to our knowledge for the first time, an extensive set of linear and nonlinear characterizations of three chalcogenide PCFs based on GeSbS and AsSe glasses including second- and third-order chromatic dispersion, effective area, losses, birefringence, nonlinear Kerr coefficient as well as Brillouin and Raman scattering properties.

II. Microstructured Chalcogenide Fibers

Chalcogenide glasses are based on sulphur, selenium, tellurium, and the addition of other elements such as arsenic, germanium, antimony, gallium, etc. They are well known for their large infrared transmission window as well as for their large nonlinearity. In this paper, we have focused our attention on three PCFs based on two compositions, which have been chosen for their great stability against crystallization effect: $Ge_{15}Sb_{20}S_{65}$ (GeSbS) for two fibers (GeSbS_1 and GeSbS_2) with two different core diameters and $As_{40}Se_{60}$ (AsSe). These glasses present any crystallization peaks in classical differential scanning calorimetry measurements (DSC).

A crucial difficulty in the fabrication of this type of fiber is to control carefully the impurity level of the starting products as well as of the final fiber. Indeed, carbon and water are frequent contaminants, especially in the case of sulphur. They must be removed from the glass batch by a combination of static and dynamic distillations. The contamination by water during the

Manuscript received October 29, 2008; revised March 25, 2009. First published May 02, 2009; current version published May 29, 2009. This work was supported in part by the Agence National de la Recherche (FUTUR project), the Conseil Regional de Bourgogne, and the Agence National de la Recherche (FUTUR project).

J. Fatome, C. Fortier, B. Kibler, S. Pitois, G. Gadret, C. Finot, and F. Smektala are with the Institut Carnot de Bourgogne, UMR 5209 CNRS-Université de Bourgogne, 21078 Dijon, France (e-mail: jfatome@u-bourgogne.fr).

T. N. Nguyen, T. Chartier, and K. Messaad are with the UMR CNRS 6082 FOTON, Laboratoire d'Optronique de l'ENSSAT, 22300 Lannion, France (e-mail: chartier@enssat.fr).

J. Troles, F. Desevedavy, and P. Houizot are with the Laboratoire Verres et Céramiques (LVC), UMR 6226 CNRS-Université de Rennes I, Campus de Beaulieu, 35042 Rennes, France (e-mail: johann.troles@univ-rennes1.fr).

G. Renversez is with the Institut Fresnel, UMR 6133 CNRS-Université Paul Cézanne Aix-Marseille III, 13397 Marseille Cedex 20, France (e-mail: gilles.renversez@fresnel.fr).

L. Brilland and N. Traynor are with PERFOS, 22300 Lannion, France (e-mail: ntraynor@perfos.com).

Digital Object Identifier 10.1109/JLT.2009.2021672

0733-8724/$25.00 © 2009 IEEE

Authorized licensed use limited to: Christophe FINOT. Downloaded on June 10, 2009 at 17:20 from IEEE Xplore. Restrictions apply.

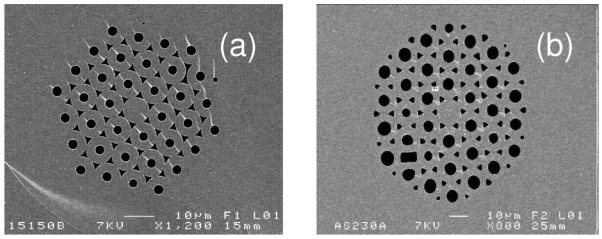

Fig. 1. (a) Cross section of GeSbS_2 PCF. (b) Cross section of AsSe PCF.

drawing step must also be avoided by using a dry drawing atmosphere. The different process steps have to be conducted at optimized temperatures to avoid any crystallization phenomenon of the glass in the bulk as well as on its surface.

The stack and draw method was used to elaborate the chalcogenide PCFs [21]. First, glass rods are realized with typical sizes around 18-cm length and around 12-mm outside diameter, respectively. The first part of the glass rod is used to draw a single index fiber which allows checking the material level of losses. The other part of this rod is then remelted to obtain the glass tube by centrifugation. Tubes around 12-mm outside diameter, about 5-mm inside diameter, and 12-cm length are then obtained by the centrifugation of the previous rod. These tubes are finally drawn down to obtain capillaries of around 600-μm outside diameter. They were then stacked in a hexagonal lattice around a central rod of the same diameter and placed into a larger jacket tube. This jacket tube is collapsed around the microstructure under depression in the furnace of the drawing tower. Parameters of furnace temperature and depression have to be adjusted to prevent any collapse of both capillary and interstitial holes. During the fabrication of tubes by centrifugation, the thermal profile is also dramatically important since the glass after its synthesis is reheated from room temperature to a temperature above the glass temperature (Tg). This is necessary to obtain a suitable viscosity for the centrifugation process but very sensitive, since atomic mobility could allow a crystallization. Another critical step is the stretching of the tube, which can lead to an alteration of the surface quality of capillaries inducing diffusion in the final fiber. The contamination by water during the drawing step must also be avoided by using a dry drawing atmosphere.

A preform for each glass composition was realized in the same experimental conditions. During the fiber drawing process, capillary holes and interstitials are maintained under positive pressure in order to obtain fibers with open interstitial holes. Indeed their presence greatly improves the fiber transmission as they enable to diminish the overlap between the guiding electric field and the interface region of capillaries where numerous scattering centres such as bubbles have already been observed [22]. Fig. 1 represents the scanning electron microscope (SEM) central region of PCFs for both considered glasses.

During the drawing, the variation of geometrical parameters of the fibers (core and holes sizes) does not exceed 2% for several meters. The uniformity of the geometry is controlled after the drawing by microscopy.

Table I gives, for the three fibers, the average of the geometrical parameters, Λ and d. The pitch Λ is the hole to hole distance and d is the hole diameter. We also report in this table the index of refraction and the transition temperature Tg for the two kind of glasses. The outer diameter of the GeSbS_1 and AsSe PCF was measured to be 125 and 280 μm for the GeSbS_2 PCF.

TABLE I
OPTICAL AND THERMAL PROPERTIES OF THE GESBS AND ASSE PCF FIBERS

Fiber	*Glass composition*	*Glass transition temperature Tg (°C)*	*Refractive index at 1,55 µm*	*Λ (µm)*	*d/Λ*
GeSbS_1	$Ge_{15}Sb_{20}S_{65}$	250	2.30	9	0.31
GeSbS_2	$Ge_{15}Sb_{20}S_{65}$	250	2.30	13.25	0.31
AsSe	$As_{40}Se_{60}$	185	2.83	7	0.42

TABLE II
MEASURED OPTICAL PROPERTIES OF THE THREE MICROSTRUCTURED CHALCOGENIDE FIBERS

Parameter	*Fiber*		
	GeSbS_1	GeSbS_2	AsSe
Λ (µm)	9	13.25	7
d/Λ	0.31	0.31	0.42
A_{eff} (μm^2)	22	50	21
α (dB/m)	5	5.5	10
D (ps/nm/km)	-421	-406	-760
S (ps/nm²/km)	0.9	1.1	2.7
DGD (ps/m)	5.5	0.8	1.24
Δn	$1.6\ 10^{-3}$	$2.4\ 10^{-4}$	$3.7\ 10^{-4}$
γ ($W^{-1}km^{-1}$)	517	227	2000
n_2 (m^2/W)	$2.8\ 10^{-18}$	$2.8\ 10^{-18}$	$1.1\ 10^{-17}$

III. PROPAGATION LOSSES

Propagation losses are of crucial importance for nonlinear phenomena, since they could dramatically reduce the interaction length to a shortest effective length of fiber defined as [29]

$$L_{\text{eff}} = \frac{1}{\alpha}\left[1 - \exp\left(-\alpha L\right)\right] \tag{1}$$

where L is the fiber length and α is the linear losses in m^{-1}.

The attenuation losses were first monitored at 1.55 μm in the 400-μm single index fibers drawn from the initial glass rod and found to be 0.5 dB/m for both GeSbS and AsSe glasses [22]. For comparison, the losses in these kinds of multimode fibers can reach 0.1 dB/m at 1.55 μm [30]. After drawing the PCFs, the propagation losses of the different fibers were then measured at 1550 nm by means of the so-called cutback technique. Experimental results as well as all optical properties of our three PCF chalcogenide fibers described thereafter are summarized in Table II. Any significant change of the physical properties has been observed between the bulk rod and the fibers. However, interfaces defects have been observed between the capillaries of the microstructure [22]. The presence of these defects explained the excess of losses observed in the PCF fibers in comparison with the material losses. The nature of the defect is not clearly identified. However, it can be bubbles and surface oxidation of the capillaries before the realization of the stack. Concerning the theoretical guiding losses, in [31], it has been demonstrated that three rings of holes are sufficient to ensure guiding losses below 1 dB/m.

Authorized licensed use limited to: Christophe FINOT. Downloaded on June 10, 2009 at 17:20 from IEEE Xplore. Restrictions apply.

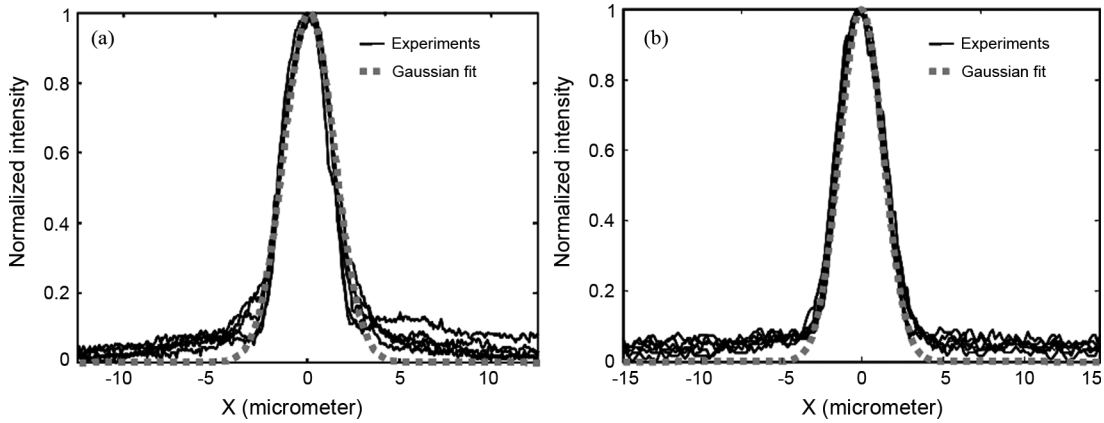

Fig. 2. Experimental traces (solid line) of the intensity distribution in the near field of (a) the GeSbS_1 fiber and (b) the AsSe fiber. Squares represent a Gaussian fit distribution.

IV. Effective Area

The effective area A_{eff} was measured at 1550 nm following a near-field method [29]. Using an adequate microscope objective, the intensity at the output of the fiber is recorded on a charge-coupled device (CCD) camera. Note that the camera is calibrated using the near field of a well-known fiber, i.e., a standard single-mode fiber. Fig. 2 gives some experimental examples (solid line) of the intensity distribution along several axes of the camera plane for the GeSbS_1 and AsSe fibers. As we can see, both fibers exhibit single-mode behavior. Indeed, for all sections, the output profiles were accurately fitted by means of a Gaussian function. Moreover, by changing injection conditions, any higher order mode was observed even for sections shorter than 10 cm. Finally, the Gaussian fit distributions of Fig. 2 (squares) allow us to determine the mode field diameter $2w_0$ (at $1/\text{e}$ intensity point) and to calculate the effective area thanks to the following formula: $A_{\text{eff}} = \pi w_0^2$.

The measured effective areas of our three PCF chalcogenide fibers are indicated in Table II.

V. Chromatic Dispersion

Measuring the chromatic dispersion of short samples of optical fibers with a reasonable accuracy has become of a major interest for the special glass optical fiber designers, manufacturers, and researchers. Various methods have been reported in the literature to measure chromatic dispersion [32]–[35]. For example, in [32] and [33], four wave mixing (FWM) and modulation instability (MI) were proved to be efficient ways to simultaneously measure the Kerr and dispersion coefficients. The variation of the time of flight of short pulses could be also used to measure the chromatic dispersion of sufficiently long fibers. In [34], the authors exploit the higher order soliton compression phenomenon in order to determine the parameters of a silica PCF fiber. But these methods often require a long length of fiber or are only suitable for the anomalous dispersion regime.

In this work, we based our dispersion measurements on an interferometric method which is able to handle short segments of optical fiber [35]. The homemade interferometric setup is illustrated in Fig. 3 and was based on a Mach–Zehnder interferometer designed with all-fibered components, thus providing both alignment simplicity and system stability. The

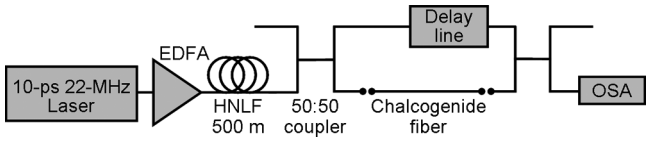

Fig. 3. Experimental setup for chromatic dispersion characterization.

reference arm was made of an integrated fibered delay line spliced to two broadband 50 : 50 couplers. The chalcogenide fiber under-test was inserted into the test path by means of a face to face clived-fiber injection setup ensured by micron precision holders. The resulting interference pattern was monitored in the frequency domain thanks to an optical spectrum analyzer (OSA). In order to measure the chromatic dispersion of our chalcogenide fibers over a wide range of wavelengths, we have first generated a supercontinuum spanning from 1100 to more than 1750 nm (OSA upper limit). The supercontinuum was obtained through the amplification and nonlinear propagation of a 10-ps pulse train into a highly nonlinear fiber (HNLF). More precisely, the picosecond-pulse train was delivered by a 22-MHz mode-locked fiber laser centered around 1553 nm, amplified at an average power of 28 dBm by means of an Erbium-doped fiber amplifier and finally injected into a 500-m-long highly nonlinear fiber (HNLF) whose parameters at 1550 nm are a chromatic dispersion $D = 0.5$ ps/km.nm, a dispersion slope $S = 0.01$ ps/km.nm^2, and a nonlinear Kerr coefficient $\gamma = 10.5\ \text{W}^{-1}.\text{km}^{-1}$. The resulting supercontinuum is illustrated in Fig. 4(a) and shows a high spectral brightness allowing measurement from 1.1 to 1.75 μm. Fig. 4(b) (solid line) shows a typical interference pattern monitored around 1550 nm where a central fringe is clearly visible. The dispersion of the fiber sample in the 1.1–1.7-μm range was then obtained by monitoring the position of this central fringe as a function of the temporal delay Δ provided by the reference arm. Experimental results (circles) are plotted in Fig. 4(c) and are well fitted by a second-order polynomial function (black solid line). The dispersion curve of our sample is then simply deduced from the delay variations by the following relation:

$$D(\lambda) = \frac{1}{Lc}\frac{d\Delta}{d\lambda}. \tag{2}$$

Authorized licensed use limited to: Christophe FINOT. Downloaded on June 10, 2009 at 17:20 from IEEE Xplore. Restrictions apply.

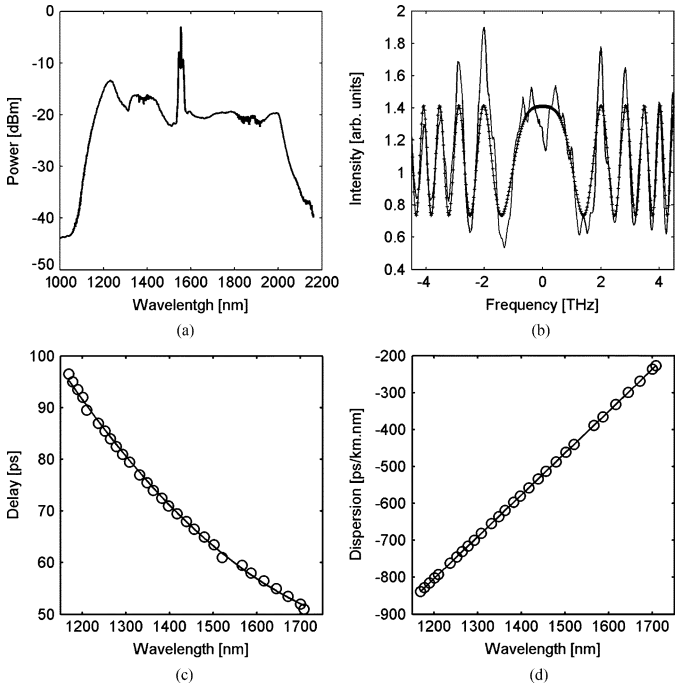

Fig. 4. (a) Supercontinuum generated at the output of the HNLF fiber. (b) Interference fringes at the coupler output. (c) Delay versus wavelength, experimental values for the $\mathrm{GeSbS\_2}$ fiber (circles), polynomial fit (solid line). (d) Dispersion versus wavelength, experimental values (circles), linear fit (solid line).

Fig. 4(d) shows the resulting dispersion curve of the GeSbS_2 chalcogenide fiber as a function of wavelength. The dispersion and dispersion slope value at 1550 nm were found to be $D = -406$ ps/nm/km and $S = dD/d\lambda = 1.1$ ps/nm^2/km. In order to validate our measurements, we have finally checked that the resulting dispersion values allowed us to retrieve the experimental interference pattern I_{int} theoretically given by

$$I_{\mathrm{int}} = I_1^2 + I_2^2 + 2\sqrt{I_1 I_2}\cos(\Phi) \tag{3}$$

where Φ is the relative phase between the two arms of the interferometer calculated thanks to the following expression:

$$\Phi = \Phi_0 + \sum_{k=1}^{\infty} \frac{(\omega-\omega_0)^k}{k!}\left(\frac{d^k\beta^{\mathrm{CHA}}}{d\omega^k}L^{\mathrm{CHA}} - \frac{d^k\beta^{\mathrm{REF}}}{d\omega^k}L^{\mathrm{REF}}\right). \tag{4}$$

In this expression, Φ_0 is a constant phase difference. β^{CHA} and β^{REF} are the mode-propagation constants of the chalcogenide fiber and reference fiber, respectively, whereas ω_0 corresponds to the optical frequency for which the temporal delay mismatch between the two arms vanishes. Fig. 4(b) (crosses) shows the theoretical interference spectrum obtained by reporting the value of D and S in expression (4) and (3). As can be seen, a good agreement is obtained between the experimental and theoretical spectra, thus validating the values of group-velocity dispersion and slope calculated from (2).

The same experiment was completed for all of the chalcogenide fibers and results at 1550 nm are indicated in Table II.

VI. Birefringence

The polarization mode dispersion properties is an important parameter for any optical signal processing function since it could induce large pulse distortion or broadening [36], [37]. In our work, the birefringence properties of the microstructured chalcogenide fibers were measured by means of the spectral-interference-based experimental setup described in Fig. 5 [38], [39]. An amplified spontaneous emission source (ASE) is passing through a polarizer (Pol) and is injected into the fiber under-test by means of the alignment option of a splicing device. At the output of the fiber, both slow and fast replicas of the signal interfere on an analyzer (A) before detection in the frequency domain thanks to an OSA [38], [39].

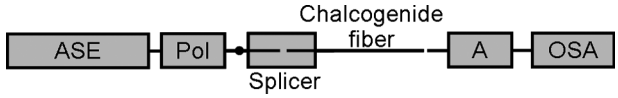

Fig. 5. Experimental setup for birefringence characterization.

Due to the first-order frequency dependence of state of polarization, a fringe-like spectrum is observed on the OSA at the output of the analyzer. More precisely, the intensity detected by the OSA is of the form [38], [39]

$$I = a + b\cos(\Delta\beta(\omega)L) \tag{5}$$

where a and b are constant coefficients which depend on the relative angle positions of input and output polarizer/analyzer. L is the length of the fiber and $\Delta\beta$ is the propagation constant difference between the slow and fast axes of the fiber which can be expanded into

$$\Delta\beta(\omega) = \Delta\beta(\omega_0) + \left(\frac{d\Delta\beta}{d\omega}\right)_{\omega_0}\Delta\omega \tag{6}$$

where $\Delta\omega = \omega - \omega_0$ is the frequency detuning with respect to the carrier frequency ω_0 of the signal. The polarization mode dispersion of the fiber is then characterized by the differential group delay (DGD) given by

$$\mathrm{DGD} = \frac{1}{Vgx(\omega_0)} - \frac{1}{Vgy(\omega_0)} = \left(\frac{d\Delta\beta}{d\omega}\right)_{\omega_0} \tag{7}$$

where Vgx and Vgy are the group velocities along the slow and fast axes, respectively.

We can see by injecting expressions (6) and (7) in (5) that the spectrum monitored on the OSA at the output of the analyzer consists of a periodic signal which fringe spacing Ω provides a direct measurement of the DGD thanks to the following relation:

$$\mathrm{DGD} = \frac{2\pi}{\Omega L}. \tag{8}$$

Fig. 6 represents a typical spectrum recorded at the output of a 0.73-m-long GeSbS_1 chalcogenide fiber sample after optimization of input and output polarizer/analyzer angle positions maximizing the fringe contrast. We can see 15 interference periods leading to a DGD of 5.5 ps/m.

Note that several irregularities appear in the interference fringes and arise from the fiber structure inhomogeneities. We have reported the experimental values of DGD in Table II as well as the optical index difference between the two axes. Typical high values around 10^{-4} were found, close to typical values of standard silica polarization maintaining fibers. More importantly, we have found a dramatic stronger birefringence

Authorized licensed use limited to: Christophe FINOT. Downloaded on June 10, 2009 at 17:20 from IEEE Xplore. Restrictions apply.

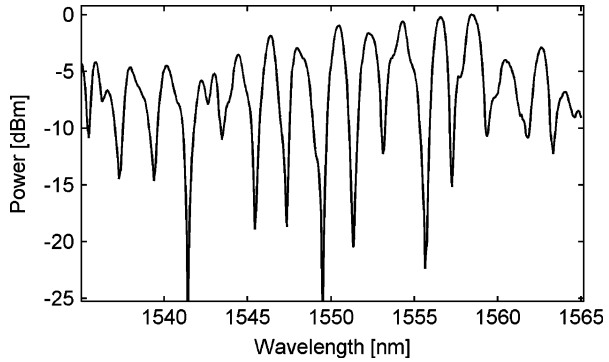

Fig. 6. Interference fringes at the chalcogenide GeSbS_1 fiber output.

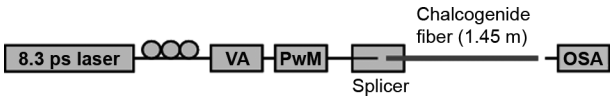

Fig. 7. Experimental setup for self-phase modulation characterization.

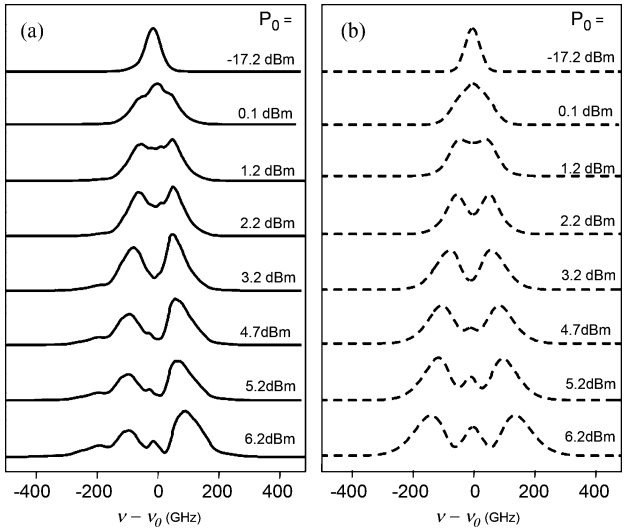

Fig. 8. (a) Experimental results: output spectra for the 1.45-m-long GeSbS_1 chalcogenide fiber as a function of input power. (b) Numerical simulations corresponding to results of (a).

for the GeSbS_1 fiber compare to the GeSbS_2 sample, which originates from the core-size reduction occurring during the drawing process and underlines the practical issue to reach symmetric microstructures of small dimensions. Previous works have already reported similar analysis showing that small silica core PCFs (large air holes and small pitch) are more sensitive to fabrication-induced asymmetries in the microstruture giving rise to higher form of birefringence that makes the polarization maintaining fiber [40]–[42]. Experimental results obtained for the three microstructured chalcogenide fibers are summarized in Table II.

VII. Self-Phase Modulation

A. Experimental Setup

In this section, we have focused our attention on the nonlinear characterization of our chalcogenide fibers. We have studied the well-known self-phase modulation effect and compare our experimental results to numerical simulations so as to deduce the Kerr nonlinear coefficient. Fig. 7 shows the experimental setup employed to characterize the nonlinear Kerr properties of the microstructured chalcogenide fibers [19], [20]. A mode-locked fiber laser generates 8.3-ps pulses at a repetition rate of 19.3 MHz around 1556 nm. The signal then passes through a polarization controller (PC) adjusted to maximize the self-phase modulation (SPM)-induced spectral broadening within the chalcogenide fiber. The signal power is controlled by a variable attenuator (VA) and measured by a power meter (PwM) before injection into the fiber under-test. Note that the input signal was coupled into the chalcogenide fiber by means of the alignment option of an optical fiber splicing device, which permits an efficient fiber coupling with losses around 2.8 dB. At the output of the fiber, the signal is finally monitored thanks to an OSA.

B. Experimental Results

Fig. 8(a) illustrates the spectra recorded at the output of the 1.45-m-long GeSbS_1 chalcogenide fiber as a function of the input average power (P_0). The values of P_0 are obtained by means of the PwM with a subtraction to the coupling loss in the splicer. Experimental results exhibit a typical self-phase modulation behavior with spectral broadening and oscillations. An asymmetry can also be observed in the output spectra, which we attribute to the initial asymmetry in the spectrum of our picosecond laser source. In order to determine the Kerr coefficient of the GeSbS_1 chalcogenide fiber, we have completed numerical simulations and compared our numerical predictions to the experimental results of Fig. 8(a). The numerical evolution of pulses was obtained by means of a split-step Fourier algorithm including experimental data of chromatic dispersion and losses. Results are plotted in Fig. 8(b) and show a good agreement with experimental results of Fig. 8(a). From these simulations, we deduced a nonlinear Kerr coefficient of $\gamma = 517\ \mathrm{W^{-1}km^{-1}}$ which is 400 times larger than a conventional single-mode fused silica fiber (SMF). The same experiment was done in the GeSbS_2 chalcogenide fiber for which the electric field is less confined by the microstructure ($A_{\mathrm{eff}} = 50\ \mu\mathrm{m}^2$) than in the GeSbS_1 fiber ($A_{\mathrm{eff}} = 22\ \mu\mathrm{m}^2$). As noted previously, the nonlinear Kerr coefficient of the GeSbS_2 fiber was deduced from the comparison between the experimental and numerical spectra and was found to be $\gamma = 227\ \mathrm{W^{-1}km^{-1}}$.

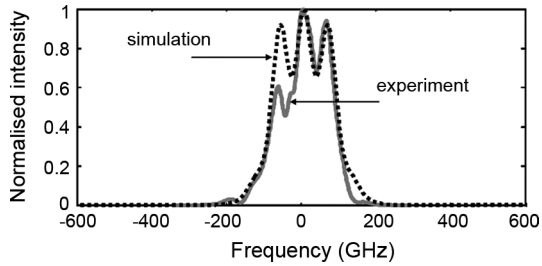

Fig. 9. Output spectrum for the 1.15-m-long AsSe chalcogenide fiber for an input average power of 1 mW; dashed line: corresponding numerical simulation.

Fig. 9 shows the experimental results obtained for the AsSe 21-$\mu\mathrm{m}^2$ chalcogenide fiber.

Authorized licensed use limited to: Christophe FINOT. Downloaded on June 10, 2009 at 17:20 from IEEE Xplore. Restrictions apply.

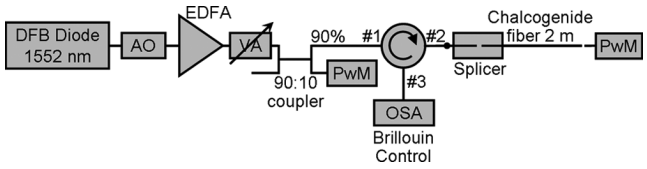

Fig. 10. Experimental setup for Brillouin characterization.

Results are similar to those of Fig. 8 and show a good agreement between the experiment and simulation. Numerical simulations provide a good estimation of the nonlinear Kerr coefficient, which was found to be $\gamma = 2000\ \mathrm{W^{-1}km^{-1}}$. One can notice, however, in both Figs. 8 and 9, that the central part of the spectrum exhibits some ripples and that some spectral pedestals have developed in the spectrum. Those features outline the strong interaction between self-phase modulation and the high dispersion of the AsSe fiber, leading to the development of the wave-breaking phenomenon [43]. Finally, the nonlinear Kerr coefficient γ and nonlinear index n_2 obtained for the three microstructured chalcogenide fibers are indicated in Table II and are quite close to the values mentioned in the literature [44]–[46], $2.4.10^{-17}\mathrm{m^2/W}$ for As_2Se_3 in [45] and $2.10^{-18}\mathrm{m^2/W}$ for $Ge_{23}Sb_{12}S_{65}$ in [46]. Note that n_2 was calculated from the Kerr coefficient following the relation [29]:

$$n_2 = \frac{\gamma \lambda A_{\mathrm{eff}}}{2\pi}. \tag{9}$$

It is important to note that the self-phase modulation induced spectrum broadening is here only limited by the effective length of the fiber (0.7 m for the GeSbS_1 PCF) and not by the dispersion length (40 m), thus underlining the critical issue of linear losses.

VIII. Brillouin Scattering Effect

The Brillouin scattering effect in step-index chalcogenide fibers has already been investigated in previous works [18], [23]–[25]. The Brillouin gain was measured to be more than 150 times larger than fused silica fiber [18], [23]–[25], which enables a high degree of integration in a host of applications such as amplification of a small optical signal [25], fiber-based lasing systems [25], or tunable delay lines via slow and fast light processes [18]. In this section, we present the experimental characterization of the Brillouin scattering occurring in the 2-m-long GeSbS_2 microstructured chalcogenide fiber [17]. Fig. 10 illustrates the experimental setup. A continuous wave (cw) is first generated at 1552 nm by means of a distributed feedback (DFB) laser diode having a spectral linewidth given by the manufacturer of 150 kHz. An acousto–optical switch (AO) converts this cw into a 140-ns quasi Gaussian pulse train at a repetition rate of 500 kHz. The pulse train is then amplified by means of an EDFA at an average power of 30 dBm. A VA, associated with a 90 : 10 coupler and a PwM, is then used to adjust the injected average power into the fiber. Finally, the resulting signal is launched into a circulator whose port #2 is used to inject the incident light into the fiber under-test by means of a splicing device and port #3 to collect the backscattered light. The intensity of the Brillouin–Stokes component is then measured at port #3 thanks to an OSA having a spectral resolution of 0.07 nm.

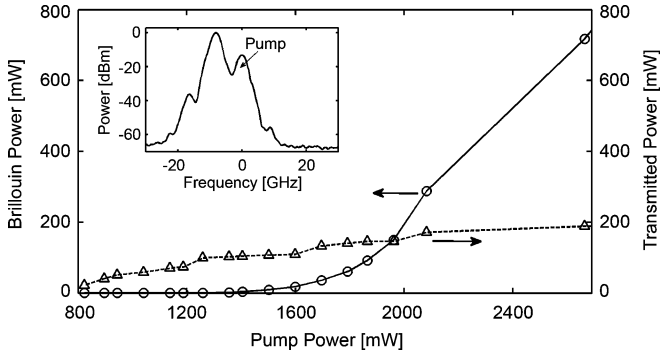

Fig. 11. Inset: experimental Brillouin spectrum recorded at port #3 of the circulator for the 2-m-long GeSbS_2 chalcogenide fiber. Backscattered and transmitted powers as a function of the input power chalcogenide fiber.

Inset in Fig. 11 shows a typical backscattered optical spectrum obtained at port #3 of the circulator. A high-power backscattered Brillouin–Stokes component is localized around -8.2 GHz which is close to the -7.95-GHz value obtained by Abedin in a single-mode As_2Se_3 fiber [23] and much lower than in a classical fused silica fiber (11 GHz) [29]. In order to determine the threshold and gain of the Brillouin scattering, we have illustrated in Fig. 11 the transmitted and backscattered Brillouin component powers as a function of the injected power. We can clearly observe a typical Brillouin behavior with an exponential growth of the amount of energy backscattered from the fiber as well as a quasi saturation of the transmitted power. The Brillouin threshold P_{th}, usually defined as the power leading to an amount of backscattered energy equal to the transmitted one [29], corresponds here to a threshold value of 1.95 W while the Brillouin gain g_B is then calculated by means of the following relation [29]:

$$\frac{g_B\, P_{th} L_{\mathrm{eff}}}{A_{\mathrm{eff}}} \approx 21 \tag{10}$$

which corresponds to a Brillouin gain of $g_B = 8.10^{-10}\mathrm{m/W}$, that is to say 100 more than in a standard silica fiber [17]. This value is smaller than those reported in [36] and [24] but could be explained by the definition of the Brillouin threshold used in these references. Finally, we have also completed the measurements by determining the linewidth of the Brillouin-gain by means of an auto-heterodyne technique [17]. The Brillouin bandwidth was found to be 9.5 MHz (versus 13 MHz for standard silica fiber) which is slightly smaller than in [36], presumably due to different glass composition and the presence of the microstructure.

IX. Raman Scattering Effect

In this section, we have focused our attention on the Raman scattering effect occurring in the GeSbS_2 microstructured chalcogenide fiber [17]. The strong nonlinear feature of the Raman process in chalcogenide fibers was previously underlined through the third-order cascaded Raman wavelength generation occurring in a step-index As_2S_3 fiber [26]. In this last work, Kulkami *et al.* have determined the Raman gain

Authorized licensed use limited to: Christophe FINOT. Downloaded on June 10, 2009 at 17:20 from IEEE Xplore. Restrictions apply.

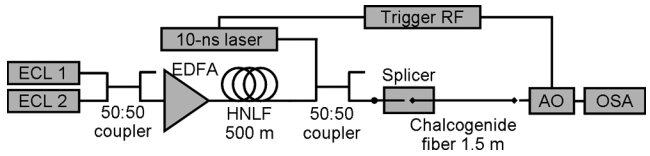

Fig. 12. Experimental setup for Raman characterization.

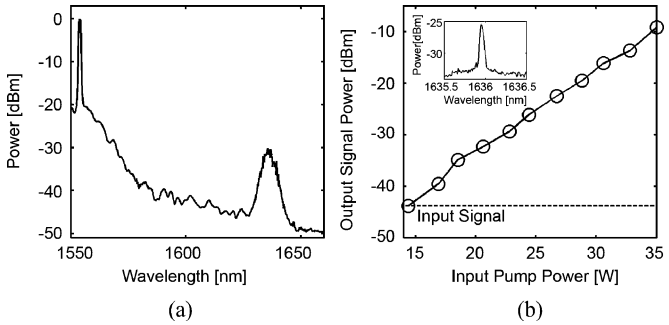

Fig. 13. (a) Spontaneous Raman scattering at the output of the GeSbS_2 chalcogenide fiber for an input pump power of 80 W. (b) Output signal power as a function of input pump power for the chalcogenide fiber. Inset: output amplified signal spectrum for a pump power of 24.5 W.

coefficient, which was found as large as ~ 89 times higher than fused silica [26]. The strong efficiency of Raman effect was also employed in order to design a chalcogenide glass Raman fiber laser [27]. On the other hand, very recently, a numerical study by Varshney *et al.* has also shown that As–Se photonic crystal fibers could increase the Raman gain efficiency by a factor four in comparison to conventional As–Se fibers [28], thus underlining the practical interest of this kind of fiber for Raman applications.

Fig. 12 shows the experimental setup used to characterize the Raman effect occurring in the GeSbS_2 microstructured chalcogenide fiber. A 1-kHz 10-ns square pulse laser emitting around 1553 nm is used as a Raman pump. In order to determine the Raman gain, we have measured the amplification undergone by a seed signal injected in a copropagating configuration and shifted from the Raman pump by 83 nm for the chalcogenide fiber (see below). The 1636-nm seed component was obtained through the generation of a broad frequency comb via the propagation of an initial 30-dBm beat signal centred around 1555 nm into a 500-m-long highly nonlinear fiber (HNLF) [47]–[49]. Note that, at the output of the fiber under-test, only the part of the signal wave which has been amplified was injected into the OSA thanks to an acousto–optic synchronized on the Raman pump.

Fig. 13(a) illustrates the spontaneous Raman response (in absence of seeding) occurring into the chalcogenide fiber for an input pump power of 80 W. The Raman detuning was measured at 83 nm (9.7 THz) with a typical FWHM of 5.5 nm. In the stimulated regime, we have measured the output power of the 1636-nm amplified signal as a function of the input Raman pump power P_{pump}. As can be seen in Fig. 13(b), a strong amplification of the input signal was observed with a maximum gain close to $G = 37$ dB. This value corresponds to a gain per unit length of 24.7 dB/m and a Raman gain of $g_{\mathrm{R}} = \ln(G).A_{\mathrm{eff}}/P_{\mathrm{pump}}.L_{\mathrm{eff}} = 1.8.10^{-11}$m/W, that is to say 180 times larger than a fused silica fiber [17] and threefold higher than the previous result reported in [26]. Finally, the inset in Fig. 13(b) illustrates a typical amplified signal spectrum recorded for a pump power of $P_{\mathrm{pump}} = 24.5$ W.

X. Conclusion

In this paper, we have investigated the linear and nonlinear properties of GeSbS and AsSe chalcogenide microstructured optical fibers. The manufactured fibers were found to have a nonlinear coefficient two order of magnitude higher than standard silica fibers as well as a Brillouin and Raman gain 100 and 180 larger than fused silica, respectively.

In order to enlarge the field of applications of this kind of fiber, for example, so as to generate supercontinuum or signal processing device around 1550 nm, a careful design of the microstructure has to be performed in order to shift the zero dispersion wavelength in the C band, and losses should be reduced thanks to a dramatic purification of the glasses whereas nonlinearity could be still enhanced by reducing the size of the core. Finally, we believe that if dimensions of the fiber are suitably designed and manufactured, chalcogenide fibers could find many applications in nonlinear optics and would be a promising candidate for ultra compact nonlinear devices.

Acknowledgment

The authors would like to thank P. Grelu and G. Millot from the Institut Carnot de Bourgogne for fruitful discussions on chromatic dispersion and birefringence measurements. They would also like to thank M. Thual and Y. Dumeige from ENSSAT of Lannion for their help on self-phase modulation measurements.

References

[1] J. C. Knight, T. A. Birks, P. S. J. Russell, and D. M. Atkin, "All-silica single-mode optical fiber with photonic crystal cladding," *Opt. Lett.*, vol. 21, pp. 1547–1549, 1996.

[2] P. S. Russell, "Photonic crystal fibers," *Science*, vol. 299, pp. 358–362, 2003.

[3] J. M. Dudley, G. Genty, and S. Coen, "Supercontinuum generation in photonic crystal fiber," *Rev. Mod. Phys.*, vol. 78, pp. 1135–1184, 2006.

[4] I. Hartl, X. D. Li, C. Chudoba, R. K. Ghanta, T. H. Ko, J. G. Fujimoto, J. K. Ranka, and R. S. Windeler, "Ultrahigh-resolution optical coherence tomography using continuum generation in an air-silica microstructure optical fiber," *Opt. Lett.*, vol. 26, pp. 608–610, 2001.

[5] S. A. Diddams, D. J. Jones, J. Ye, T. Cundiff, J. L. Hall, J. K. Ranka, R. S. Windeler, R. Holzwarth, T. Udem, and T. W. Hanch, "Direct link between microwave and optical frequencies with a 300 THz femtosecond laser comb," *Phys. Rev. Lett.*, vol. 84, pp. 5102–5105, 2000.

[6] P. Petropoulos, T. M. Monro, W. Belardi, K. Furusawa, J. H. Lee, and D. J. Richardson, "$2R$-regenerative all-optical switch based on a highly nonlinear holey fiber," *Opt. Lett.*, vol. 26, pp. 1233–1235, 2001.

[7] F. Benabid, J. Knight, and P. Russell, "Particle levitation and guidance in hollow-core photonic crystal fiber," *Opt. Exp.*, vol. 10, pp. 1195–1203, 2002.

[8] B. Shaw, P. Thielen, F. Kung, V. Nguyen, J. Sanghera, and I. Aggarwal, "IR supercontinuum generation in As-Se photonic crystal fiber," in *Tech. Dig. Adv. Solid-State Photon.*, Mar. 2007, paper TuC5.

[9] N. Sugimoto, T. Nagashima, T. Hasegawa, S. Ohara, K. Taira, and K. Kikuchi, "Bismuth-based optical fiber with nonlinear coefficient of 1360 $\mathrm{W^{-1}km^{-1}}$," presented at the Opt. Fiber Commun. Conf., Anaheim, CA, Mar. 2004, postdeadline paper PDP26.

Authorized licensed use limited to: Christophe FINOT. Downloaded on June 10, 2009 at 17:20 from IEEE Xplore. Restrictions apply.

[10] J. H. V. Price, T. M. Monro, H. Ebendorff-Heidepriem, F. Poletti, P. Horak, V. Finazzi, J. Y. Y. Leong, P. Petropoulos, J. C. Flanagan, G. Brambilla, M. Feng, and D. J. Richardson, "Mid-IR supercontinuum generation from nonsilica microstructured optical fibers," *IEEE J. Sel. Top. Quantum Electron.*, vol. 13, pp. 738–749, 2007.

[11] P. Domachuk, N. A. Wolchover, M. Cronin-Golomb, A. Wang, A. K. George, C. M. B. Cordeiro, J. C. Knight, and F. G. Omenetto, "Over 4000 nm bandwidth of Mid-IR supercontinuum generation in sub-centimeter segments of highly nonlinear tellurite PCFs," *Opt. Exp.*, vol. 16, pp. 7161–7168, 2008.

[12] T. Nagashima, T. Hasegawa, S. Ohara, and N. Sugimoto, "Dispersion shifted Bi_2O_3-based photonic crystal fiber," presented at the Eur. Conf. Opt. Commun., Cannes, France, Sep. 2006, paper We1.3.2.

[13] D. Pelusi, F. Luan, E. Magi, M. R. Lamont, D. J. Moss, B. J. Eggleton, J. S. Sanghera, L. B. Shaw, and I. D. Aggarwal, "High bit rate all-optical signal processing in a fiber photonic wire," *Opt. Exp.*, vol. 16, pp. 11506–11512, 2008.

[14] D. Yeom, E. C. Mägi, M. R. E. Lamont, M. A. F. Roelens, L. Fu, and B. J. Eggleton, "Low-threshold supercontinuum generation in highly nonlinear chalcogenide nanowires," *Opt. Lett.*, vol. 33, pp. 660–662, 2008.

[15] M. Pelusi, V. G. Ta'eed, L. Fu, E. C. Mägi, M. R. E. Lamont, S. Madden, D.-Y. Choi, D. A. P. Bulla, B. Luther-Davies, and B. J. Eggleton, "Applications of highly-nonlinear chalcogenide glass devices tailored for high-speed all-optical signal processing," *IEEE J. Sel. Top. Quantum Electron.*, vol. 14, no. 3, pp. 529–539, May–Jun. 2008.

[16] P. Petropoulos, H. Ebendorff-Heidepreim, V. Finazzi, R. C. Moore, K. Frampton, D. J. Richardson, and T. M. Monro, "Highly nonlinear and anomalously dispersive lead silicate glass holey fibers," *Opt. Exp.*, vol. 11, pp. 3568–3573, 2003.

[17] C. Fortier, J. Fatome, S. Pitois, F. Smektala, G. Millot, J. Troles, F. Desevedavy, P. Houizot, L. Brilland, and N. Traynor, "Experimental investigation of Brillouin and Raman scattering in a 2SG sulfide glass microstructured chalcogenide fiber," *Opt. Exp.*, vol. 16, pp. 9398–9404, 2008.

[18] K. Y. Song, K. S. Abedin, K. Hotate, M. González Herráez, and L. Thévenaz, "Highly efficient Brillouin slow and fast light using As_2Se_3 chalcogenide fiber," *Opt. Exp.*, vol. 14, pp. 5860–5865, 2006.

[19] L. B. Fu, M. Rochette, V. G. Ta'eed, D. J. Moss, and B. J. Eggleton, "Investigation of self-phase modulation based optical regeneration in single mode As_2Se_3 chalcogenide glass fiber," *Opt. Exp.*, vol. 13, pp. 7639–7646, 2005.

[20] L. Fu, V. G. Ta'eed, E. C. Mägi, I. C. M. Littler, M. Pelusi, M. R. E. Lamont, A. Fuerbach, H. C. Nguyen, D. I. Yeom, and B. J. Eggleton, "Highly nonlinear chalcogenide fibres for all-optical signal processing," *Opt. Quantum Electron.*, vol. 39, pp. 1115–1131, 2008.

[21] L. Brilland, F. Smektala, G. Renversez, T. Chartier, J. Troles, T. N. Nguyen, N. Traynor, and A. Monteville, "Fabrication of complex structures of holey fibers in chalcogenide glasses," *Opt. Exp.*, vol. 14, pp. 1280–1285, 2006.

[22] L. Brilland, J. Troles, P. Houizot, F. Désévédavy, Q. Coulombier, G. Renversez, T. Chartier, T. N. Nguyen, J. L. Adam, and N. Traynor, "Interfaces impact on the transmission of chalcogenides photonic crystal fibres," *J. Ceramic Soc. Jpn.*, vol. 116, pp. 1024–1027, 2008.

[23] K. S. Abedin, "Observation of strong stimulated Brillouin scattering in single-mode As_2Se_3 chalcogenide fiber," *Opt. Exp.*, vol. 13, pp. 10266–10271, 2005.

[24] C. Florea, M. Bashkansky, Z. Dutton, J. Sanghera, P. Pureza, and I. Aggarwal, "Stimulated Brillouin scattering in single-mode As_2S_3 and As_2Se_3 chalcogenide fibers," *Opt. Exp.*, vol. 14, pp. 12063–12070, 2006.

[25] K. S. Abedin, "Brillouin amplification and lasing in a single-mode As_2Se_3 chalcogenide fiber," *Opt. Lett.*, vol. 31, pp. 1615–1617, 2006.

[26] O. P. Kulkarni, C. Xia, D. J. Lee, M. Kumar, A. Kuditcher, M. N. Islam, F. L. Terry, M. J. Freeman, B. G. Aitken, S. C. Currie, J. E. McCarthy, M. L. Powley, and D. A. Nolan, "Third order cascaded Raman wavelength shifting in chalcogenide fibers and determination of Raman gain coefficient," *Opt. Exp.*, vol. 14, pp. 7924–7930, 2006.

[27] S. D. Jackson and G. Anzueto-Sanchez, "Chalcogenide glass Raman fiber laser," *Appl. Phys. Lett.*, vol. 88, p. 221106, 2006.

[28] S. K. Varshney, K. Saitoh, K. Iizawa, Y. Tsuchida, M. Koshiba, and R. K. Sinha, "Raman amplification characteristics of As_2Se_3 photonic crystal fibers," *Opt. Lett.*, vol. 33, pp. 2431–2433, 2008.

[29] G. P. Agrawal, *Nonlinear Fiber Optics*, 3rd ed. Boston, MA: Academic, 2001.

[30] G. G. Devyatyk, M. F. Churbanov, I. V. Schripatchev, G. E. Snopatin, E. M. Dianov, and V. G. Ploticheńko, "Recent development in As-S glass fibres," *J. Non Crystalline Solids*, vol. 256 & 257, pp. 318–322, 1999.

[31] J. Troles, L. Brilland, F. Smektala, P. Houizot, F. Desevedavy, Q. Coulombier, N. Traynor, T. Chartier, T. N. Nguyen, J. L. Adam, and G. Renversez, "Chalcogenide microstructured fibers for infrared systems, elaboration modelization, and characterization," *Fiber Integrated Opt.*, vol. 28, pp. 11–26, 2009.

[32] H. Chen, "Simultaneous measurements of non-linear coefficient, zero-dispersion wavelength and chromatic dispersion in dispersion-shifted fibers by four-wave mixing," *Opt. Commun.*, vol. 220, pp. 331–335, 2003.

[33] J. Fatome, S. Pitois, and G. Millot, "Measurement of nonlinear and chromatic dispersion parameters of optical fibers using modulation instability," *Opt. Fiber Technol.*, vol. 12, pp. 243–250, 2006.

[34] T. N. Nguyen, T. Chartier, M. Thual, P. Besnard, L. Provino, A. Monteville, and N. Traynor, "Simultaneous measurement of anomalous group-velocity dispersion and nonlinear coefficient in optical fibers using soliton-effect compression," *Opt. Commun.*, vol. 278, pp. 60–65, 2007.

[35] F. Koch, S. V. Chernikov, and J. R. Taylor, "Dispersion measurement in optical fibers over the entire spectral range from 1.1 μm to 1.7 μm," *Opt. Commun.*, vol. 175, pp. 209–213, 2000.

[36] J. P. Gordon and H. Kogelnik, "PMD fundamentals: Polarization mode dispersion in optical fibers," *Proc. Nat. Acad. Sci. USA*, vol. 97, pp. 4541–4550, 2000.

[37] J. Garnier, J. Fatome, and G. Le Meur, "Statistical analysis of pulse propagation driven by polarization-mode dispersion," *J. Opt. Soc. Amer. B*, vol. 19, pp. 1968–1977, 2002.

[38] X. D. Cao and D. D. Meyerhofer, "Frequency-domain interferometer for measurement of the polarization mode dispersion in single-mode optical fibers," *Opt. Lett.*, vol. 19, pp. 1837–1839, 1994.

[39] G. Millot and J. M. Dudley, "Polarization mode dispersion measurement in high-birefringence fibers by means of stimulated Raman scattering," *Appl. Opt.*, vol. 41, pp. 2589–2591, 2002.

[40] I. K. Hwang, Y. J. Lee, and Y. H. Lee, "Birefringence induced by irregular structure in photonic crystal fiber," *Opt. Exp.*, vol. 11, pp. 2799–2806, 2003.

[41] K. L. Reichenbach and C. Xu, "The effects of randomly occurring nonuniformities on propagation in photonic crystal fibers," *Opt. Exp.*, vol. 13, pp. 2799–2807, 2005.

[42] L. Labonte, D. Pagnoux, P. Roy, F. Bahloul, and M. Zghal, "Numerical and experimental analysis of the birefringence of large air fraction slightly unsymmetrical holey fibres," *Opt. Commun.*, vol. 262, pp. 180–187, 2006.

[43] C. Finot, B. Kibler, L. Provost, and S. Wabnitz, "Beneficial impact of wave-breaking or coherent continuum formation in normally dispersive nonlinear fibers," *J. Opt. Soc. Amer. B*, vol. 25, pp. 1938–1948, 2008.

[44] T. Cardinal, K. A. Richardson, H. Shim, A. Schulte, R. Beatty, K. Le Foulgoc, C. Meneghini, J. F. Viens, and A. Villeneuve, "Non-linear optical properties of chalcogenide glasses in the system As-S-Se," *J. Non Crystalline Solids*, vol. 256 & 257, pp. 353–360, 1999.

[45] R. E. Slusher, G. Lenz, J. Hodelin, J. Sanghera, L. B. Shaw, and I. D. Aggarwal, "Large Raman gain and nonlinear phase shifts in high-purity As_2Se_3 chalcogenide fibers," *J. Opt. Soc. Amer. B*, vol. 21, pp. 1146–1155, 2004.

[46] L. Petit, N. Carlie, K. Richardson, A. Humeau, S. Cherukulappurath, and G. Boudebs, "Nonlinear optical properties of glasses in the system Ge/Ga-Sb-S/Se," *Opt Lett.*, vol. 31, pp. 1495–1497, 2006.

[47] C. Fortier, B. Kibler, J. Fatome, C. Finot, S. Pitois, and G. Millot, "All-fibered high-quality low duty-cycle 160-GHz femtosecond pulse source," *Laser Phys. Lett.*, vol. 5, pp. 817–820, 2008.

[48] C. Finot, J. Fatome, S. Pitois, and G. Millot, "All-fibered high-quality low duty-cycle 20-GHz and 40-GHz picosecond pulse sources," *IEEE Photon. Technol. Lett.*, vol. 19, no. 21, pp. 1711–1713, Nov. 1 2007.

[49] J. Fatome, S. Pitois, and G. Millot, "320/640 GHz high-quality pulse sources based on multiple four-wave mixing in highly nonlinear optical fibre," *Electron. Lett.*, vol. 41, pp. 1391–1392, 2005.

Authorized licensed use limited to: Christophe FINOT. Downloaded on June 10, 2009 at 17:20 from IEEE Xplore. Restrictions apply.

Julien Fatome was born in Charleville-Mézières, France, in 1978. After graduating from the engineering school of ESIREM, Dijon, France, he received the DEA degree and the Ph.D. degree in physics for studies of ultrashort pulse propagation at 160-Gb/s in dispersion managed optical fiber lines from the University of Bourgogne, Dijon, France, in 2000 and 2004, respectively.

In 2005, he became CNRS Research Engineer at the Institut Carnot de Bourgogne, Department of Physics, University of Bourgogne. He is author or coauthor of more than 60 publications and conference papers. He is currently carrying out research in nonlinear effects and pulse trains propagation at ultrahigh bit rate in optical fibers.

Coraline Fortier, photograph and biography not available at the time of publication.

Thanh Nam Nguyen was born in Phutho, Vietnam, in 1980. He received the Ph.D. degree in the field of optical communication and physics science from the University of Rennes 1, France, in 2008.

Currently, he is a Researcher at FOTON Laboratory, ENSSAT, Lannion, France, and a Lecturer at Posts and Telecommunications Institute of Technology, Hanoi, Vietnam. His research interests are nonlinear characterization in optical fiber and nonlinear applications of fiber in the telecommunications, especially in all optical regeneration.

Thierry Chartier was born in 1969. He received the Ph.D degree in physics from the Université de Rennes 1, France, in 1997.

In 1998, he joined the laboratory CORIA of Université de Rouen to study high-power fiber lasers. In 2003, he joined the laboratory FOTON, Lannion, France, where his research activities concern nonlinear optics in fibers for telecommunication systems and fiber lasers.

Frederic Smektala was born in 1966. He received the Ph.D degree in materials chemistry from the University of Rennes, France, in 1992.

He developed research on nonsilica glasses and optical infrared fibers. He has published more than 80 papers in the field. Currently, he works more particularly on the nonlinear optical properties of chalcogenide glasses and fibers, especially in the photonic crystal fibers configuration. He was a Professor at Rennes University from 2002 to 2006. He moved to the University of Bourgogne, Dijon, France, in 2006, where he is now a Professor at the Institut Carnot de Bourgogne, UMR 5209 CNRS-Université de Bourgogne.

Khalida Messaad, photograph and biography not available at the time of publication.

Bertrand Kibler, photograph and biography not available at the time of publication.

Stephane Pitois, photograph and biography not available at the time of publication.

Gregory Gadret, photograph and biography not available at the time of publication.

Christophe Finot, photograph and biography not available at the time of publication.

Johann Troles, photograph and biography not available at the time of publication.

Frederic Desevedavy, photograph and biography not available at the time of publication.

Patrick Houizot, photograph and biography not available at the time of publication.

Gilles Renversez, photograph and biography not available at the time of publication.

Laurent Brilland, photograph and biography not available at the time of publication.

Nicholas Traynor, photograph and biography not available at the time of publication.

Authorized licensed use limited to: Christophe FINOT. Downloaded on June 10, 2009 at 17:20 from IEEE Xplore. Restrictions apply.